Effects of Oxygen Inhibition and Post-Processing on Exposure Controlled Projection Lithography Process Accuracy

Ying Zhang, Amit Jariwala*, David W. Rosen

George W. Woodruff School of Mechanical Engineering

Georgia Institute of Technology

Atlanta, Georgia, 30332

*Corresponding author. Tel.: +1 404 894 3931 Email: Amit.jariwala@gatech.edu

Abstract

Exposure Controlled Projection Lithography (ECPL) is a mask-projection stereolithography process which can be used to create micro lenses on flat or curved substrates. In the ECPL process, the ultraviolet light patterned by the dynamic mask passes through a transparent substrate to cure the photopolymer resin to a certain shape. The dimensions of the part can be controlled by the exposure time and functional pixels in the dynamic mask. In this paper, a modified process planning method is presented with the considerations of post-processing and oxygen inhibition, which can vary part dimensions significantly. The effects of post-processing and oxygen inhibition are studied and characterized. The accuracy of the lateral and vertical dimensions of the cured part are improved by the revised method. Experimental validation is obtained by fabricating samples using the ECPL system.

1. Introduction

Exposure Controlled Projection Lithography (ECPL) is an additive manufacturing process where components are solidified in a photopolymer resin by ultraviolet light. The ECPL process is a similar system as the Masked Projection Stereolithography process (MPSLA) [1] except that the curing of the photopolymer resin occurs by passing light energy through a transparent substrate. With control of the light intensity profile and curing time, the vertical shape of the sample will be fabricated instead of layer-by-layer approach used in Stereolithography (SLA) process. The dimension of the sample can be controlled by the exposure time and functional pixels in the projector. To project functional pixels, a series of binary bitmap images are used. Recently researchers such as Erdmann et al. [2] and Mizukami et al. [3] have developed similar techniques as the ECPL process. However, the knowledge of controlling the process to achieve high accuracy and precision in the final cured shape was not presented.

The revised process planning method to control the lateral dimensions of the cured part in the ECPL process with consideration of a ray tracing model and photopolymerization kinetic model was presented by Jariwala et.al.[4]. The cured results showed a significant deviation with simulation results in dimensions. Therefore, a hypothesis was developed by Jariwala et.al [5] that the effect of oxygen diffusion and inhibition should be considered during the polymerization process. The revised process planning method provided better control of the curing results.

However, the accuracy was still not satisfied and the model was not suitable for all cases. In order to improve the accuracy, a similar process planning method with revised rate constant was presented by Jariwala et.al [5]. A unique process planning approach was demonstrated which simulated the empirical models in the COMSOL software package and then formulated in MATLAB software to simulate the entire curing process. With the experimentally validated rate constant, the error between simulation and experiments was still around 15%.

In this paper, rate constants were revised again with experimental validation. The irradiance model was modified to fit the experimental data. Furthermore, the effect of post-washing process was studied and reduced to an insignificant level. The revised process planning approach is presented and results demonstrate significant improvements in part dimensional accuracy.

2. ECPL System

Figure 1 shows the block diagram of the ECPL process. As the block diagram indicates, the process model of the ECPL system contains three main parts: apply energy, process and post-process. To apply energy, the ultra violet light source apply through the beam expander to expand the laser beam diameter. Then the light passes through the diffuser to enlarge the diameter and homogenize the beam's intensity and the collimating lens to collimate the light. After that, the UV coated mirror will be used to direct the light on a dynamic mask, which is the DMD projection system. The projection system is used to enlarge or reduce the image presented on the DMD and project it on the resin chamber. The part is cured in the resin chamber, which consists of two glass slides and a spacer which is shown in Figure 2. The uncured monomer resin is loaded inside.

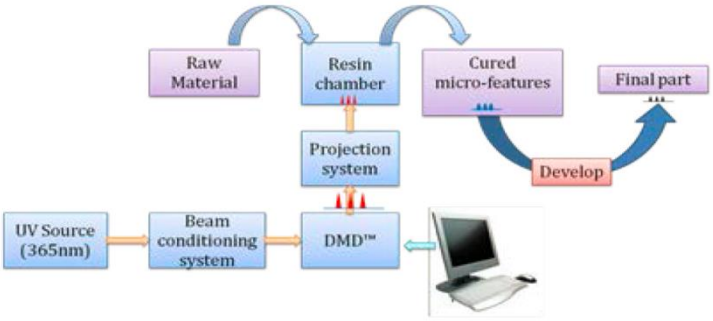

Figure 1: Block diagram of ECPL system [9]

3. Existing ECPL Process Background

3.1. Irradiance Model

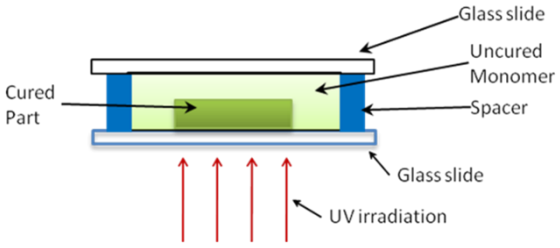

Figure 2: Schematic of the resin chamber [9]

The ECPL system is analytically modeled in two phases – Irradiance Model and Photopolymerization Model. The irradiance model models the irradiance received by the resin in terms of the process parameters and is presented in detail in Jariwala et al. [6]. The UV Light energy is the primary energy source in the ECPL system. The total amount of energy is controlled by the exposure time and by the size of the irradiated region, given by the size of the projected bitmaps. The exposure (units of energy/area) is referred as the total amount of UV energy incident per unit area. The total dose of energy provided to the resin is regulated by the distribution of irradiance at the substrate level. The relationship between the irradiance distribution on the DMD chip and the substrate of the resin chamber was investigated as the irradiance model in Jariwala et al. [6]. The irradiance

model can be validated by placing a camera at the substrate level. Figure 3 shows the comparison of simulation results from the irradiance model with experimental data (irradiance detected by the camera). The result demonstrates that the irradiance model can estimate the actual exposure profile on the substrate level though there were small deviations, which might be due to the misalignment of optics or the resolution difference between the simulation model and UV CCD camera.

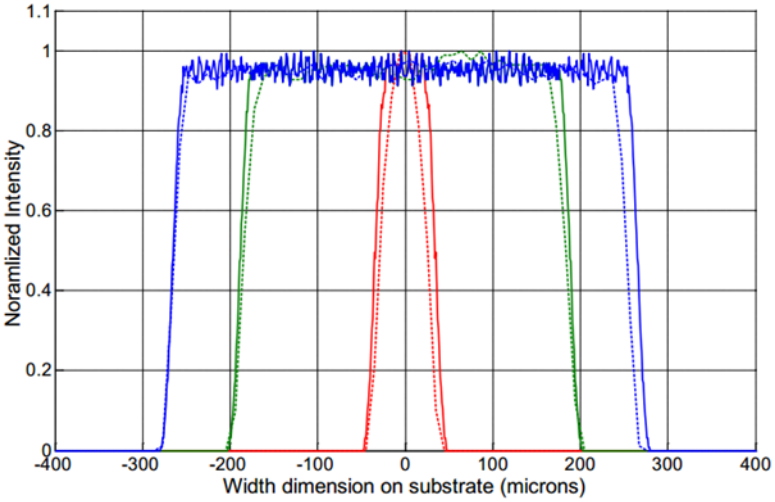

Figure 3: Comparison of simulation results from Irradiance model (solid lines) with data from Camera (dashed lines). Red corresponds to 10pixels; green to 60pixels and blue to 90pixels [9]

3.2. Polymerization Model

Photopolymerization is the reaction of monomers or macromers to produce solid polymeric structures by light-induced initiation and polymerization [7]. Most Stereolithography (SL) resins contain acrylate monomers. For an acrylate resin system, the usual catalyst is a free radical. In Stereolithography, the radical is generated photo chemically. The source of the photo chemically generated radical is a photo initiator, which reacts with an actinic photon. This produces radicals that catalyze the polymerization process. According to Beer-Lambert's law of absorption, the exposure (mJ/cm^2) decreases exponentially with depth [8].

$$\mathrm{E(z)} = E_{max} e^{\frac{-z}{Dp}} \tag{1}$$

where D_p is the resin "penetration depth" (a resin parameter) at the given wavelength and E_{max} is the exposure at the surface of the resin ($z = 0$). Z is the cured part height. Based on experimental observations, this model was modified in [3, 4] as follows:

$$\mathrm{z} \approx D_{ps} * \ln\left(\frac{DpL}{D_{PS}} * \frac{E}{E_c} + 1 - \frac{DpL}{D_{PS}}\right) \tag{2}$$

where E_c is the critical exposure (exposure threshold that induces photopolymerization), D_{PL} is the penetration depth through liquid resin, and D_{PS} is the penetration depth through solid resin. The parameters E_c, D_{pL} and D_{pS} are usually fit to experimental data at a specific resin composition and cure intensity. Moreover, this empirical model was found not to be adequate to predict the actual reaction inside the resin. The diffusion effects of oxygen were investigated to have significant effects on the size, shape and properties of parts fabricated by Stereolithography [9] and were incorporated into the kinetic model of the ECPL system. The model incorporates the chemical reaction inside the resin with oxygen diffusivity. The polymerization kinetic model is presented briefly as follows. The concentrations of photoinitiator [In], radicals [$R\cdot$], unreacted double bonds [DB], and oxygen [O_2] were modeled in the kinetic model. The reactions

considered by them were as follows [10]. When the photopolymer resin receives light energy, the photoinitiator absorbs it and decomposes into two radicals with first order rate constant of K_d,

$$\ln \xrightarrow{\text{Kd}} 2\text{R}\cdot \tag{3}$$

The initiator decomposition rate, *Kd*, is well known in literature and is modeled as a function of the local intensity, which varies with depth (following the Beer-Lambert Law) [11]

$$K_d = \frac{2.3\Phi\varepsilon\lambda}{N_A hc} I_0 e^{(-2.3\varepsilon[In]z)} \tag{4}$$

where $0<\phi<1$ is the quantum efficiency of the photoinitiator, N_A is Avagadro's number, h is Planck's constant, and c is the speed of light. The molar absorptivity of the resin, ε, depends upon the source wavelength λ. The depth inside the resin is z. The kinetic equation of the initiator can then be given as,

$$\frac{d[In]}{dt} = -K_d[In] \tag{5}$$

The radicals can then react with the double bonds to form longer chains, or form a dead radical or be quenched with dissolved oxygen as depicted by the following three equations.

$$\text{R}\cdot + DB \xrightarrow{Kp} R\cdot \tag{6}$$

$$\text{R}\cdot + \text{R}\cdot \xrightarrow{Kt} R_{dead} \tag{7}$$

$$\text{R}\cdot + O_2 \xrightarrow{K_{t,O_2}} R_{dead} \tag{8}$$

R_{dead} is species produced that destroys one or more radicals. The rate constants used are K_p for propagation of a radical through an acrylate double bond, K_t for termination between two radicals, and $K_{t,O2}$ for termination of a radical with an oxygen molecule. R* is non-propagating radicals.

The overall rate of initiator decomposition, *Ri*, is modeled by multiplying the rate constant K_d by the initiator concentration [*In*]

$$R_i = K_d[In] \tag{9}$$

The kinetic equations for the double bond [*DB*], live radicals [*R*·] and oxygen [O_2] can be given as follows:

$$\frac{d[\text{R}\cdot]}{dt} = 2k_d I(z)[In] - 2k_d[\text{R}\cdot]^2 - k_{t,O_2}[\text{R}\cdot][O_2] \tag{10}$$

$$\frac{d[DB]}{dt} = -k_p[\text{R}\cdot][DB] \tag{11}$$

$$\frac{\partial[O_2]}{\partial t} = -k_{t,O_2}[\mathrm{R}\cdot][O_2] + D_{O_2}\frac{\partial^2[O_2]}{\partial z^2} \quad (12)$$

The effect of oxygen inhibition and diffusion was explicitly modeled in Eq. 12. Due to the high diffusivity of dissolved oxygen in the photopolymer resin, it was assumed that the oxygen would primarily diffuse from uncured top layers of the sample chamber down to the curing front, competing with double bonds for radicals and significantly slowing down the rate at which the double bonds are converted, thus increasing the gel time. This equation was modified to account for oxygen diffusion in two dimensions as shown in Eq. 13.

$$\frac{\partial[O_2]}{\partial t} = -k_{t,O_2}[\mathrm{R}\cdot][O_2] + D_{O_2}\frac{\partial^2[O_2]}{\partial x^2} + D_{O_2}\frac{\partial^2[O_2]}{\partial z^2} \quad (13)$$

The researchers estimated the rate constants, K_t, K_p & $K_{t,O2}$ by fitting the simulation results with the experimental data from Fourier-transform infrared (FTIR) experiments[9]. They had suggested that the individual rate constants are not unique and may vary. Since the FTIR experiments were conducted at 100 times the intensity of the light used in the ECPL system, it is possible that the effect of oxygen inhibition and diffusion was not adequately captured using the presented rate constants. Hence, these constants were varied to suit the ECPL experimental conditions. Constant rates used for the current system will be specified in the section 5.

3.3. Process Plan Formulation

The existing process planning methods for ECPL system are discussed in Jariwala et al.[9] In this work, process planning is used to estimate the exposure times and corresponding bitmaps for the desired part shape and dimensions. MATLAB and COMSOL software are used in the process planning. Part shape and dimensions are provided as inputs. The process planner first estimates the bitmap and exposure time for the first layer. Then, the program will connect with COMSOL to modify the time by simulating the effects such as oxygen inhibition and diffusion. After that it will calculate the exposure time for next layers in the same method. The flowchart for estimating the first set of process inputs and subsequent set of process inputs are shown in Figures 4 and 5, respectively. With reference to Figure 4, the first bitmap and exposure time were estimated by optimizing the cured part edge. It is to be noted that the primary function of the first bitmap is not to cure the entire part geometry, but to cure the base and the corresponding edge of the desired part. For the subsequent layer process shown in Figure 5, the inputs are the bitmap for the first "layer" and the corresponding exposure time and the desired cured part geometry. The dotted lines show the simultaneous dependence of the optimization module on the system module and the material module. The dashed lines show the iterative nature of the loop and the process stops when the entire desired part geometry is cured completely (within a pre-set threshold).

4. Revised Irradiance Model

The existing irradiance model has been demonstrated to be able to predict the exposure profile on the substrate level very well. Experimental validation was also reported in Jariwala et al [8]. However, the experimental validation was provided by projecting a large pixel size bitmap with 5, 10 and 30 seconds exposure time. As Figure 6 shows, the top region of the irradiance

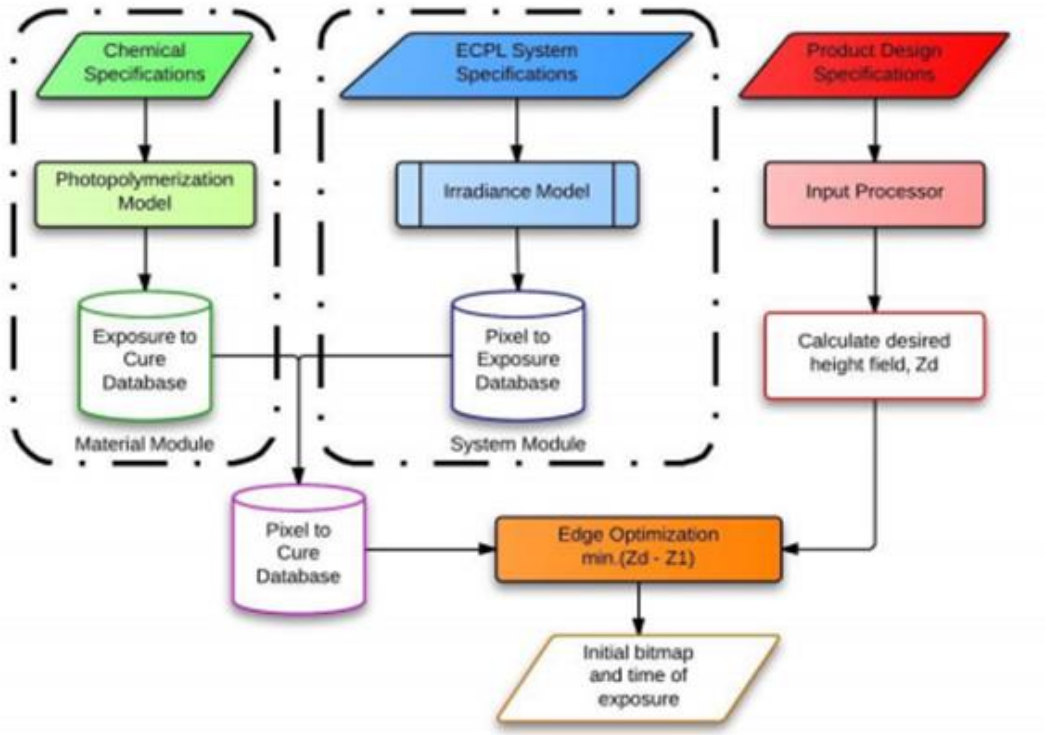

Figure 4: Flowchart for estimating first set of process inputs [9]

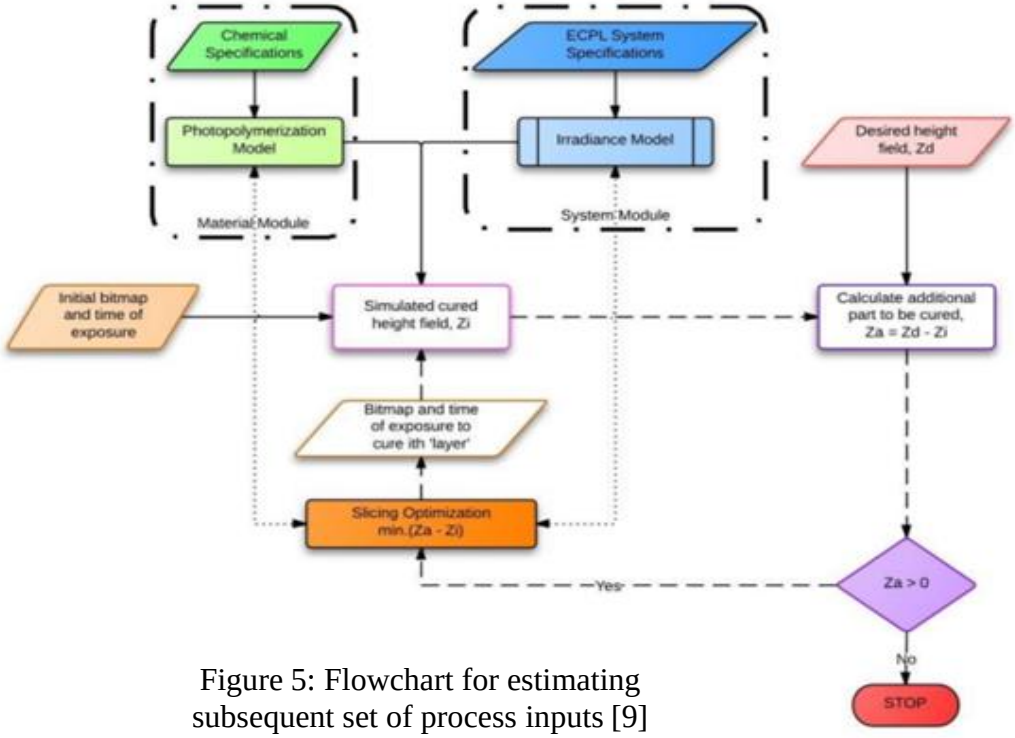

Figure 5: Flowchart for estimating subsequent set of process inputs [9]

model has much more variation than the bottom part, which means that for small amount of curing time, the irradiance model can not estimate the exposure profile to a high degree of accuracy. It will work for cylindrical parts which have no limitations in curvature. However, for

spherical lens and aspheric lens, the curing time for each "layer" will be less than 2 seconds, which will induce more difference between the simulation results and experimental results. Figure 7 is an aspheric lens example of the experimental results. The figure shows that the dimensional error between simulation and experiment increases with the decreasing desired height which is also related to the exposure time. Hence, the irradiance model needs to be improved to fit the experimental data. Figure 8 shows the comparison of revised irradiance model and previous irradiance model. The blue lines show the old irradiance model and the red lines indicate the new irradiance model.

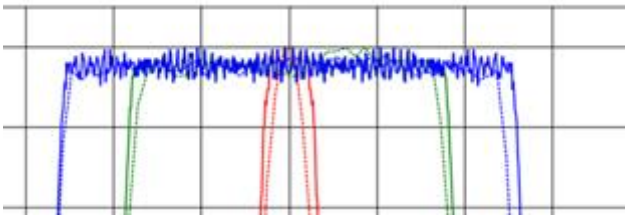

Figure 6: cropped view of the top region of Figure 3

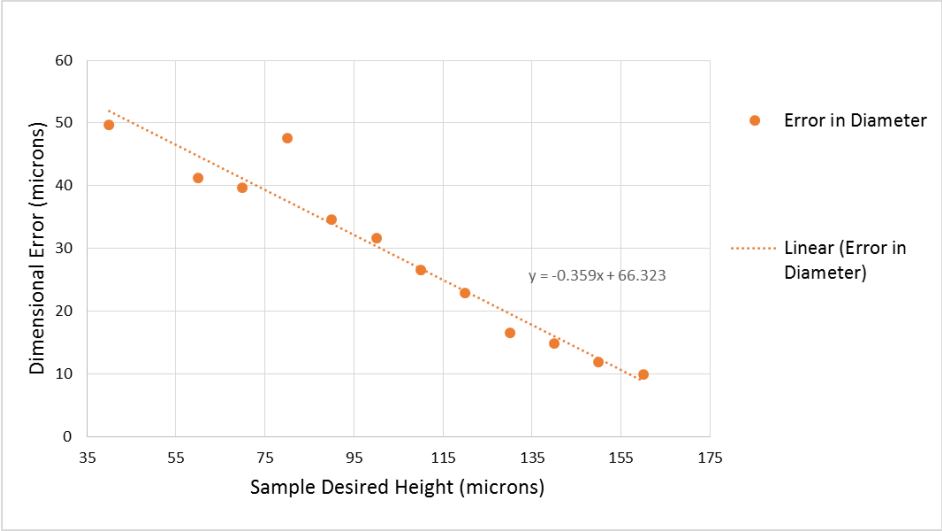

Figure 7: Dimensional error vs. sample height

5. Revised Rate Constant

In our previous work, significant differences were observed between simulation results and fabricated parts, as shown in Figure 9. Cross-sectional profiles of cured parts as obtained from 3D laser confocal microscopy are plotted along with simulated part profiles. All samples were exposed at the same intensity for an exposure time of 30s with different pixel size. Results suggest that parts with large diameters can reach the same height for the same amount of exposure time, but for small diameter parts, the reached heights decrease with decreasing diameter. Simulation results cannot accurately predict the case.

With a new UV source, the UV light intensity was changed from 140 to 210 W/m^2. Due to this change, new rate constants for propagation and termination were fit to data measured from part fabrication experiments. The physical parameters, experimental conditions and the fitted rate constants in the study are presented in Table 1. In addition to the change in UV intensity, it

was found that the intensity was not stable in the lab, so the light intensity is measured every time before doing experiments.

Evan after this work, it was observed that the rate constants shown in Table 1 only worked for the large pixel bitmaps (greater than approximate 200 μm in diameter). Therefore, to fabricate accurate small parts, process plans have to be manually modified. The process is well understood enough that such manual modifications do enable simulation results to match the experimental results.

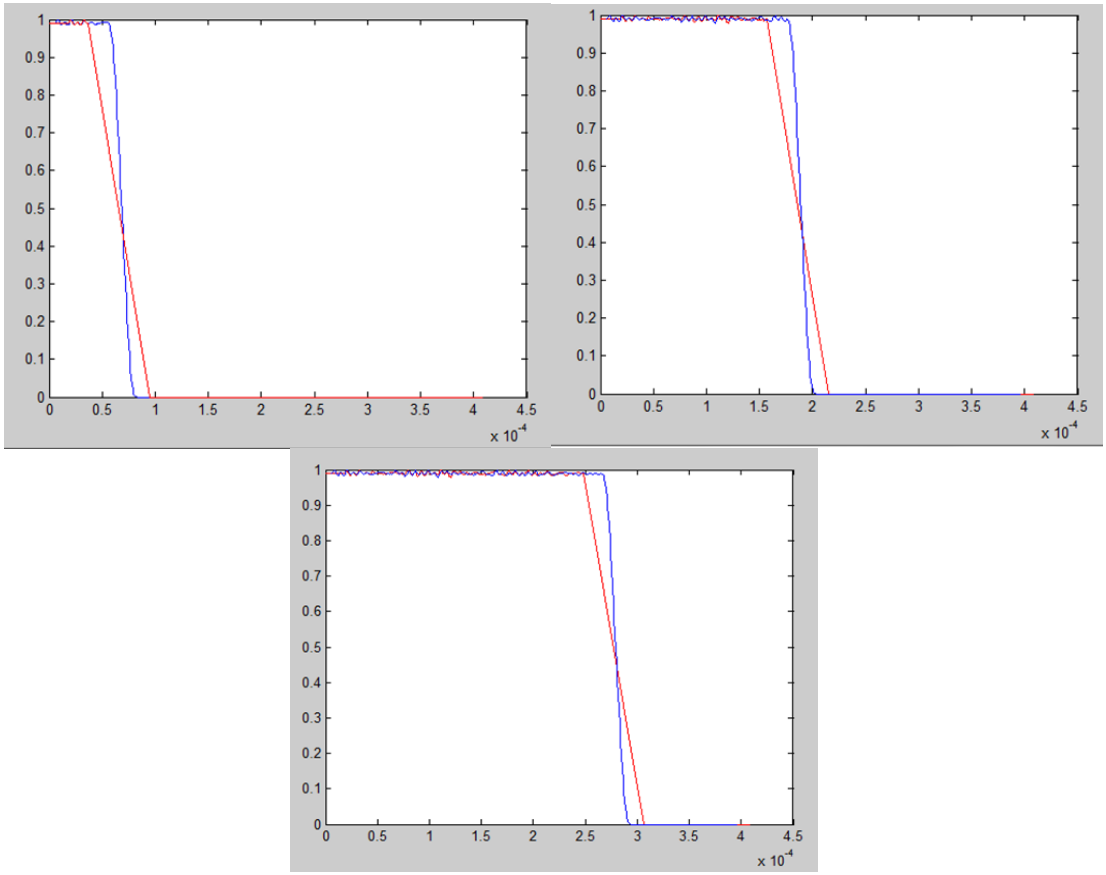

Figure 8: Examples of revised irradiance model

6. Effect of Post Processing

The post-process is referred as washing process in the ECPL system. It is used to transform the cured part into a finished product. After the cured part is fabricated, the cured sample is still submerged to the uncured resin in the resin chamber. The uncured resin needs to be removed by gently washing. An inappropriate washing method can lead to damage of the cured gel boundary and also the surface of the sample. The washing method developed in the ECPL system is to use a solution of water and Triton-X to gently remove all traces of uncured monomer, and then apply water to clear the surface. Various solvents such as acetonitrile, hexane, ethyl acetate and a solution of water and soap were also tried. The solution of water and Triton-X (soap solution) is found to be the most effective and repeatable way to clean the samples. As

Figure 10 shows, a good washing method can provide a clear, smooth and clean surface, but for bad washing methods, the surface is very rough and looks like a moon face. However, the current washing method will still wash off partial cured resin. The outside layer of the sample will be sticky and easily to be removed especially for smaller samples based on the experiments. Therefore, in order to reduce the effect of post processing, a dimensional adjustment will be applied before inputting the design specification into the process planning program.

Table 1: Physical parameters used in this study

Parameter	**Value**	**Units**	**Source**
Quantum efficiency of radical, Φ	0.6	-	[17]
Molar absorptivity of photons at 365nm wavelength, ε	15	m^2/mol	[17,18]
UV light Intensity, I_0	210	W/m^2	experimental
Molecular weight of Monomer, TMPTA	296	g/mol	Sartomer
Molecular weight of Photoinitiator, DMPA	256	g/mol	Ciba
Rate constant for propagation reaction, Kp	1.66	m^3/mol-s	Modified from [15]
Rate constant for termination reaction, Kt	1.31	m^3/mol-s	Modified from [15]
Rate constant for termination via oxygen quenching, $K_{t,O2}$	125	m^3/mol-s	Modified from [15]
Diffusion coefficient of Oxygen, D_{O2}	1.00E-10	m^2/s	[19]
Initial concentraton of Oxygen, $[O_2]_0$	1.05	mol/m^3	[20]

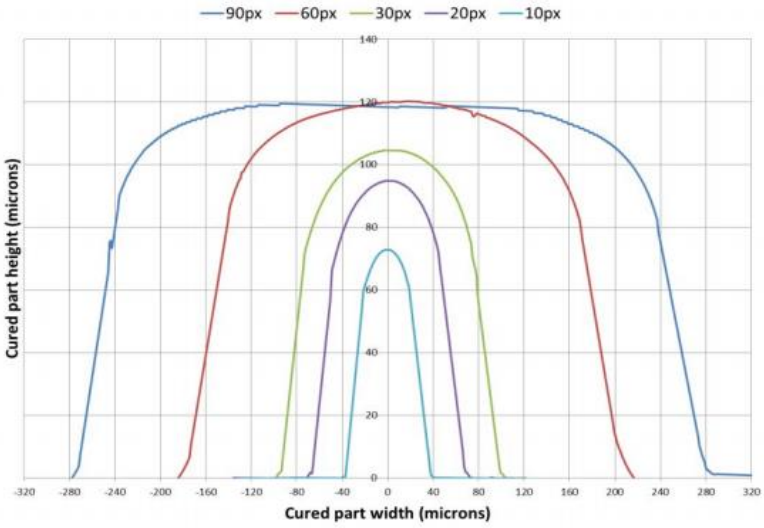

Figure 9: Different pixels with the same amount of exposure time [12]

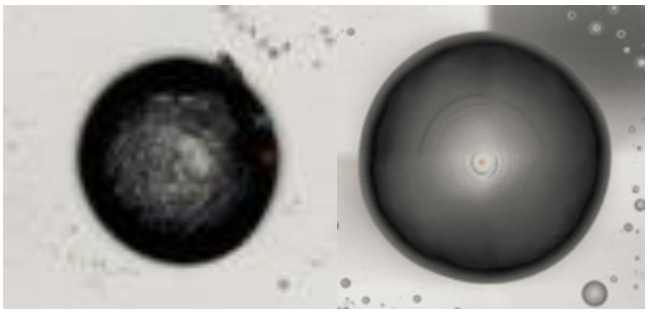

Figure 10: Sample surface with good post processing (right) and bad post processing method (left)

7. Experimental Validation

A set of 42 different part shapes and sizes were investigated in order to test the revised process planning method. This set contains both cylindrical and aspheric parts with diameters ranging from 200 to 590 μm and heights ranging from 60 to about 122 μm. In Section 7.2, one specific case of an aspheric lens is investigated in detail.

7.1 Set of Cylindrical and Aspheric Parts

In order to validate the process planning method with revised irradiance model, revised rate constant and consideration of the effect of the post processing, a large number of cylindrical and aspheric parts were fabricated and measured. Matlab scripts were written to encode the revised process planning algorithm. The bitmaps and exposure time will be obtained after entering the desired geometry. By projecting the bitmaps through the ECPL system, samples were fabricated, then washed and measured using the LEXT 3D confocal microscope. The experiments and results are presented in Appendix A. In our case, the geometry height and diameter were mainly focused. The desired part height and width, experimental height and width, error between the simulation and experiment in both height and diameter and the error percentage were listed in the table. One sample from the table will be investigated in the following section.

7.2 Test Case

The desired geometry is an aspheric lens with 200 micrometers in diameter and 65 micrometers in height. The conic constant is -1. After running the process planner on this geometry, the bitmaps and exposure times were computed, as shown in Figure 11.

The experimental results are shown in Figure 12. A 20X microscope objective was used to obtain the dimensional height and diameter, but measured points along the profile had significant noise. Therefore, the 50X microscope objective was used to get the geometry profiles. The figure shows the comparison of desired geometry and experimental result in half-sectional view.

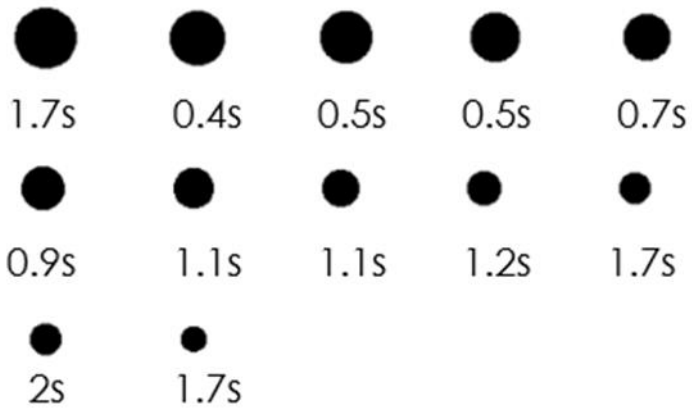

Figure 11: Bitmaps used in the test case

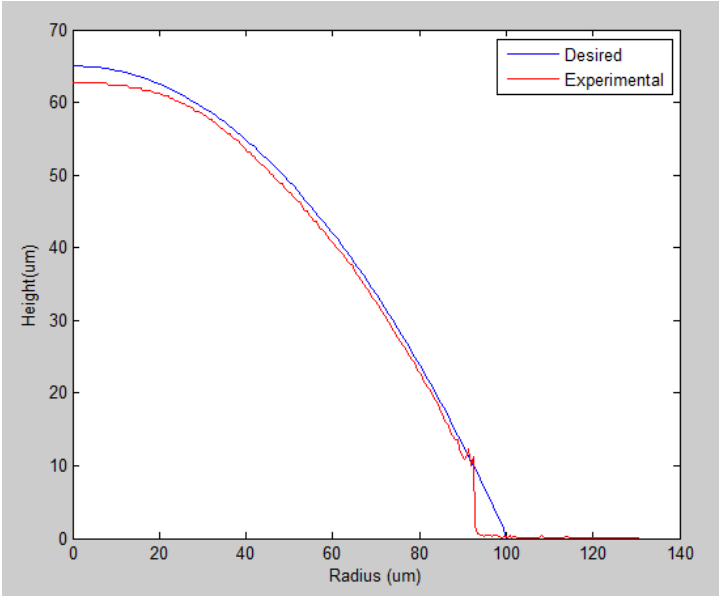

Figure 12: Comparison of the half-sectional profiles of the cured part sample and the desired part geometry

It was observed that the experimental result matched the desired geometry very well. The cut-off edge error, between 90 and 100 μm in the graph, was likely caused by microscope measurement problems associated with steep part geometry. We can see the edge clearly when the other objective was used.

Overall, from the entire table in Appendix A, compared to the previous published results [9], it can be concluded that the current revised processing method with the consideration of the oxygen inhibition and post processing yields much better results. The deviation of part height between the simulation and experiment is less than 10% and the deviation in the diameter is less than 5% which was expected.

8. Conclusion

This paper presented a revised process planning method for the ECPL mask-projection stereolithography process with the consideration of oxygen inhibition and post processing. The rate constants of the polymerization model and irradiance model were modified according to the experimental data. By using COMSOL and MATLAB software to simulate the ECPL process, the bitmaps and exposure time which are needed to cure the desired geometry were obtained. As all the experimental result demonstrate, the simulated height and diameter can predict the experimental result fairly well. The error is less than 10% in the height and 5% in the diameter.

In order to reduce the error percentage to our demands: less than 5% in both dimension, future improvement need to be investigated. Due to the limitation of the COMSOL, neural network may be used to set up the statistic model to get better results.

Acknowledgment

This material is based upon work supported by the National Science Foundation under Grant No. CMMI-1234561. Any opinions, findings, and conclusions or recommendations expressed in this publication are those of the authors and do not necessarily reflect the views of the National Science Foundation.

References

[1] Limaye A. and Rosen D., 2007, "Process Planning Method for Mask Projection MicroStereolithography", *Rapid Prototyping Journal,* **13**(2), pp. 76-84

[2] Erdmann L., Deparnay A., Maschke G., Längle M., Bruner R., 2005, "MOEMS-Based Lithography for the Fabrication of Micro-Optical Components", *Journal of Microlithography, Microfabrication, Microsystems,* **4**(4), pp. 041601-1, -5.

[3] Mizukami Y., Rajnaik D., Rajnaik A., Nishimura M., 2002, "A Novel Microchip for Capillary Electrophoresis with Acrylic Microchannel Fabricated on Photosensor Array", *Sensors and Actuators B,* **81**, pp. 202-209.

[4] Jariwala A., Ding F., Zhao X., Rosen D., 2008, "A Film Fabrication Process on Transparent Substrate Using Mask Projection Stereolithography", D. Bourell, R. Crawford, C. Seepersad, J. Beaman, H. Marcus, eds., *Proceedings of the 19th Solid FreeformFabrication Symposium,* Austin, Texas, pp. 216-229.

[5] Jariwala A., Ding F., Boddapati A., Breedveld V., Grover M. A., Henderson C. L., Rosen D. W., 2011, "Modeling effects of oxygen inhibition in mask-based Stereolithography", *Rapid Prototyping Journal,* **17**(3), pp. 168-175.

[6] Jariwala, A., Ding, F., Zhao, X., & Rosen, D. W., "A Process Planning Method for Thin Film Mask Projection Micro-Stereolithography", *Proceedings of the ASME 2009 International Design Engineering Technical Conferences & Computers and Information in Engineering Conference.* San Diego, CA, Paper no. DETC2009-87532, 2009.

[7] Decker, C., "Photoinitiated Curing of Multifunctional Monomers", *Acta Polymer, 43,* pp. 333-347, 1994.

[8] Gibson, I, Rosen, D.W., Stucker, B., *Additive Manufacturing Technologies: Rapid Prototyping to Direct Digital Manufacturing,* Second Edition, Springer, 2015. ISBN: 978-1-4939-2113-3..

[9] Jariwala A., Jones H., Kwatra A., Rosen D. W., 2013, "Process Planning Method For Exposure Controlled Projection Lithography", *Proceedings of the 24th Solid Freeform Fabrication Symposium,* Austin, Texas, pp. 95-110.

[10] Boddapati A., Rahane S., Slopek R., Breedveld V., Henderson C., and Grover M., "Gel time prediction of multifunctional acrylates using a kinetics model," Polymer, vol. 52, pp. 866-873, 2011.

[11] Boddapati, A., "Modeling Cure Depth during Photopolymerization of Multifunctional Acrylates", M.S. Thesis, Georgia Institute of Technology, School of Chemical & Biomolecular Engineering, Atlanta, 2010.

[12] Jariwala, A. S., & Rosen, D. "Modeling and process planning for exposure controlled projection lithography", P.H.D Thesis, Georgia Institute of Technology, School of Mechanical Engineering, Atlanta, 2015.

Appendix A: Experimental data with different desired geometry

Desired Diameter (um)	200	200	200	200	200	200	200	200	200	200	200	200	200	200
Experimetal Diameter (um)	193.662	191.146	194.403	195.242	200.274	197.758	196.178	197.855	189.371	193.565	191.468	191.887	192.854	192.3705
Error in Diameter (um)	6.338	8.854	5.597	4.758	-0.274	2.242	3.822	2.145	10.629	6.435	8.532	8.113	7.146	7.6295
relative error percent in Diameter(%)	3.169	4.427	2.7985	2.379	-0.137	1.121	1.911	1.0725	5.3145	3.2175	4.266	4.0565	3.573	3.81475
Desired Height (um)	60	60	60	65	65	65	65	65	70	70	70	80	80	80
Experimetal Height (um)	58.977	58.142	56.341	61.129	61.265	61.197	62.919	63.129	65.545	64.166	63.3555	72.353	72.252	72.3025
Error in Height (um)	1.023	1.858	3.659	3.871	3.735	3.803	2.081	1.871	4.455	5.834	6.6445	7.647	7.748	7.6975
relative error percent in Height (%)	1.705	3.096667	6.098333	5.955385	5.746154	5.850769	3.201538	2.878462	6.364286	8.334286	9.492143	9.55875	9.685	9.621875
Desired Diameter (um)	300	300	300	300	300	300	300	300	300	300	300	300	300	300
Experimetal Diameter (um)	289.245	288.407	289.966	289.611	292.482	299.192	285.736	286.736	295.17	296.008	288.446	288.446	289.285	289.285
Error in Diameter (um)	10.755	11.593	10.034	10.389	7.518	0.808	14.264	13.264	4.83	3.992	11.554	11.554	10.715	10.715
relative error percent in Diameter(%)	3.585	3.864333	3.344667	3.463	2.506	0.269333	4.754667	4.421333	1.61	1.330667	3.851333	3.851333	3.571667	3.571667
Desired Height (um)	60	60	70	70	80	80	80	80	90	90	90	90	100	100
Experimetal Height (um)	57.9	57.119	69.031	67.449	78.005	78.499	75.2	77.523	91.106	89.345	85.783	86.384	94.191	93.616
Error in Height (um)	2.1	2.881	0.969	2.551	1.995	1.501	4.8	2.477	-1.106	0.655	4.217	3.616	5.809	6.384
relative error percent in Height (%)	3.5	4.801667	1.384286	3.644286	2.49375	1.87625	6	3.09625	1.228889	0.727778	4.685556	4.017778	5.809	6.384
Desired Diameter (um)	300	300	396	396	400	400	400	400	574	574	582	582	590	590
Experimetal Diameter (um)	289.285	293.285	396.213	391.181	417.182	407.117	418.085	419.698	577.381	577.381	594.994	596.672	615.124	608.414
Error in Diameter (um)	10.715	6.715	-0.213	4.819	-17.182	-7.117	-18.085	-19.698	-3.381	-3.381	-12.994	-14.672	-25.124	-18.414
relative error percent in Diameter(%)	3.571667	2.238333	0.053788	1.216919	4.2955	1.77925	4.52125	4.9245	0.589024	0.589024	2.232646	2.520962	4.258305	3.121017
Desired Height (um)	110	100	82.12	82.12	107.5	107.5	121.6	121.6	82.24	82.24	107.6	107.6	121.8	121.8
Experimetal Height (um)	103.156	90.695	79.918	79.402	100.711	100.688	112.552	113.677	83.184	83.77	107.787	109.573	123.813	124.59
Error in Height (um)	6.844	9.305	2.202	2.718	6.789	6.812	9.048	7.923	-0.944	-1.53	-0.187	-1.973	-2.013	-2.79
relative error percent in Height (%)	6.221818	9.305	2.681442	3.309791	6.315349	6.336744	7.440789	6.515625	1.14786	1.860409	0.173792	1.833643	1.652709	2.29064